

Thorough Representation of Thermal Conductivity of Group VA Puckered Monolayer Structures with a Single Parameter

Tuğbey Kocabaş

*Department of Advanced Technologies, Graduate School of Sciences,
Anadolu University, Eskisehir, TR 26555, Turkey*

Deniz Çakır

Department of Physics and Astrophysics, University of North Dakota, Grand Forks, North Dakota 58202, USA

Oğuz Gülseren

Department of Physics, Bilkent University, Bilkent, Ankara 06800, Turkey

Feridun Ay and Nihan K Perkgöz

*Department of Electrical and Electronics Engineering,
Faculty of Engineering, Anadolu University, Eskisehir, TR 26555, Turkey*

Cem Sevik

*Department of Mechanical Engineering, Faculty of Engineering,
Anadolu University, Eskisehir, TR 26555, Turkey**

Emergence of new two dimensional materials open a new avenue for applications, such as thermoelectricity, based on their astonishing thermal properties. In this respect, lattice thermal transport properties of group VA elements (P, As, Sb, PAs, PSb, AsSb) with black phosphorus like puckered structure are systematically investigated by first principles density functional theory based calculations. In spite of the apparent differences in vibrational properties of these materials, we establish an intriguing correlation between the lattice thermal conductivity, κ , of all the considered materials. Notably, a single parameter function, $\kappa(T) = \alpha \times \kappa_{ref}(T)$, well predicts the thermal conductivity of other group VA monolayers using only the thermal conductivity of any reference system ($\kappa_{ref}(T)$), for example phosphorene, as an input, where α is a constant. As expected, phosphorene has the highest thermal conductivity due to its low atomic mass. As a matter of course, anisotropy in relaxation times and phonon group velocities give rise to anisotropic thermal properties, and degree of anisotropy decreases as the mass of constituent atom(s) increases. In addition, the contribution of ZA mode ($< 50\%$) to the thermal conductivity is markedly small as compared to graphene ($\sim 80\%$), and decreases as the average atomic mass in the unit cell increases. We also reveal that thermal conductivity of P, As and Sb monolayers scales as inverse square of atomic mass (i.e. $\kappa \sim 1/m^2$). Moreover, our calculations on alloyed structures clearly resemble that thermoelectric potential of these materials can be improved by suppressing its thermal properties.

PACS numbers:

I. INTRODUCTION

Triggered by the rediscovery of black phosphorus (BP), group VA materials, specifically monolayer arsenic (As) and antimony (Sb), have started to receive attention due to their peculiar thermal, optical and electronic properties¹⁻⁶. In fact, this excitement among different researchers is inspired by the fabrication of first phosphorene (P monolayer) based transistor in 2014⁷. The interest not only spreads to the optical and electronic community but also to the research groups studying thermal properties^{2,8-10}. From the optical and electronic points of view, phosphorene is appealing because of its high carrier mobility and direct band gap¹¹. This band gap is also found to vary from 0.3 eV to 2 eV progressively when its thickness is reduced from its bulk form to single-layer form. On the other hand, the relatively low thermal conductivity and its directional dependency due to the

anisotropic lattice structure in particular for phosphorene (P monolayer) and arsenene (As monolayer) is of immense value for thermoelectric applications, providing higher electro-thermal conversion efficiency^{2,8,12}. Hence, the materials with such properties present a high potential to start a new line of research and development leading to completely new technologies.

Group VA elements have the electronic configuration of s^2p^3 in the outermost shell, where this sp^3 bonding causes a non-planarity, either a puckered or buckled structure^{9,13,14}. Van der Waals forces hold the 2D layers where each atom in a layer is 3-fold coordinated with covalent bonds¹⁵. The puckered structure of P, As, and Sb have been reported to be thermodynamically stable with high electron/hole mobility¹⁶ and low thermal conductivity¹⁷ values, which is essential for high-performance innovative thermoelectric research. Therefore, it is very motivating to spend more intense theoretical effort on the nature of phonon transport in these

materials in order to shed light on their lattice thermal transport properties. In addition, low thermal conductivity of the VA column inspires controlling the thermal transport properties by material engineering such as using the alloys of these elements. Hence, in this study, it is also an object of interest regarding the change in thermal conductivity when Group VA elements are alloyed.

Therefore, we calculate the intrinsic lattice thermal conductivity of six single layer two dimensional structures of P, As, Sb, PAs, PSb, and AsSb with space group symmetries as $Pmna$ (53) and $Pmn2_1$ (31), by solving the phonon Peierls-Boltzmann transport equation (BTE) based on first-principles calculations, in this research work.

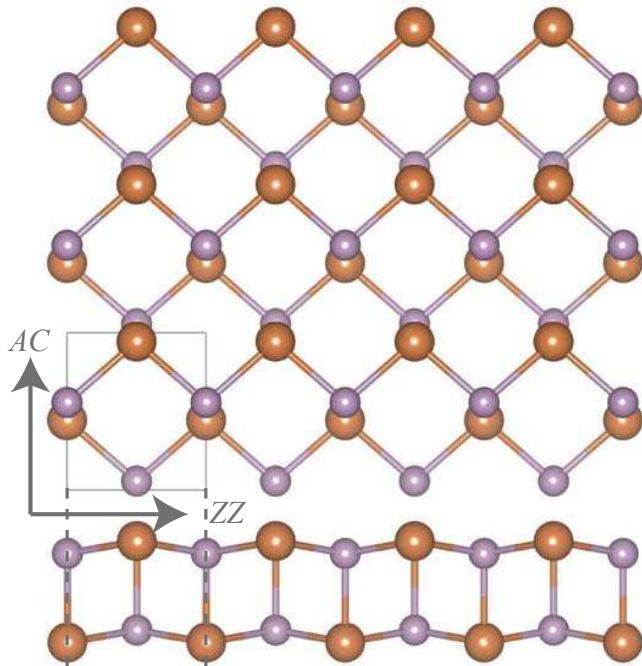


FIG. 1: Top and side views of the considered structures. Here, monatomic unit cells include four P, As, or Sb atoms and diatomic structures includes two from each as shown.

II. METHOD

The structural and dynamical properties of all the considered systems are predicted by first-principles calculations based on density functional-theory (DFT) and density-functional perturbation theory (DFPT), as implemented in the Vienna Ab initio Simulation package (VASP) code¹⁸⁻²⁰. The exchange-correlation interactions are treated using the generalized gradient approximation (GGA) within the Perdew-Burke-Ernzerhof (PBE) formulation^{21,22}. The single electron wave functions are expanded in plane waves with kinetic energy cutoff of 450 eV. For the structure optimizations, the Brillouin-zone integrations are performed using a Γ -centered regular $10 \times 8 \times 1$ k -point mesh within the Monkhorst-Pack

scheme²³. The convergence criterion for electronic and ionic relaxations are set as 10^{-7} eV and 10^{-3} eV/Å, respectively. In order to minimize the periodic interaction along the z -direction the vacuum space between the layers is taken at least 15 Å.

Lattice thermal transport properties are determined by the self-consistent solution of Peierls-Boltzmann transport equation²⁴ as implemented in ShengBTE code^{25,26}. The zeroth iteration solutions corresponding to Relaxation Time Approximation (RTA) are also predicted in order to clarify the influence of the quasi-momentum-conserving normal and the non-quasi-momentum-conserving Umklapp scattering processes on thermal transport results. The second-order inter-atomic force constants (IFCs) required by the ShengBTE code are obtained by PHONOPY code which extracts the proper force-constant file from the results predicted by DFPT as implemented in VASP. The third-order IFCs are derived from the VASP calculations of the structures generated by considering up to twelve next-nearest-neighbor interactions. Here, $6 \times 6 \times 1$ and $5 \times 4 \times 1$ supercell structures are used in the DFT calculations performed to predict the second- and third-order IFCs, respectively. In lattice thermal transport calculations $70 \times 48 \times 1$ well converged q -grid and 5.36 Å^{27,28} out of plane lattice constant, d are used for all the considered single layer materials.

III. RESULTS

As seen in Fig. 1, the primitive unit cell of the considered systems is a rectangular lattice with a four-atom basis and a space group of $Pmna$ for P and As and $Pmn2_1$ for Sb, PAs, PSb and AsSb. Therefore, except for the three acoustic modes involving the in-phase vibrations of atoms in the unit cell, out-of-phase vibrations of the atoms give rise to nine optical modes for all the structures. The calculated phonon dispersions corresponding to these vibrational modes of the six group VA monolayer crystals are depicted in Fig. 2, in which the group velocity for each q point is also represented as line color. First of all, we observe no appreciable negative frequencies, indicating that these monolayer structures are thermodynamically stable at $T=0$ K. The in-plane longitudinal acoustic (LA) and transverse acoustic (TA) modes of all the materials have a linear dependence on the wavevector, whereas out-of-plane acoustic or flexural modes (ZA) have a quadratic dependence in the long wavelength limit as extensively observed in two-dimensional materials such as graphene. The considered six compounds display similar dispersion curves but with distinctive Debye frequencies which results in different phonon group velocity ($v_{qi} = \frac{\partial \omega_{qi}}{\partial q}$) values. Namely, the maximum frequency (ω_m) values at the Γ -point changes as $\omega_{m,P} > \omega_{m,As} > \omega_{m,Sb}$ and $\omega_{m,PAs} > \omega_{m,PSb} > \omega_{m,AsSb}$, mainly due to the bond stiffness, different atomic masses for pristine monolayers and re-

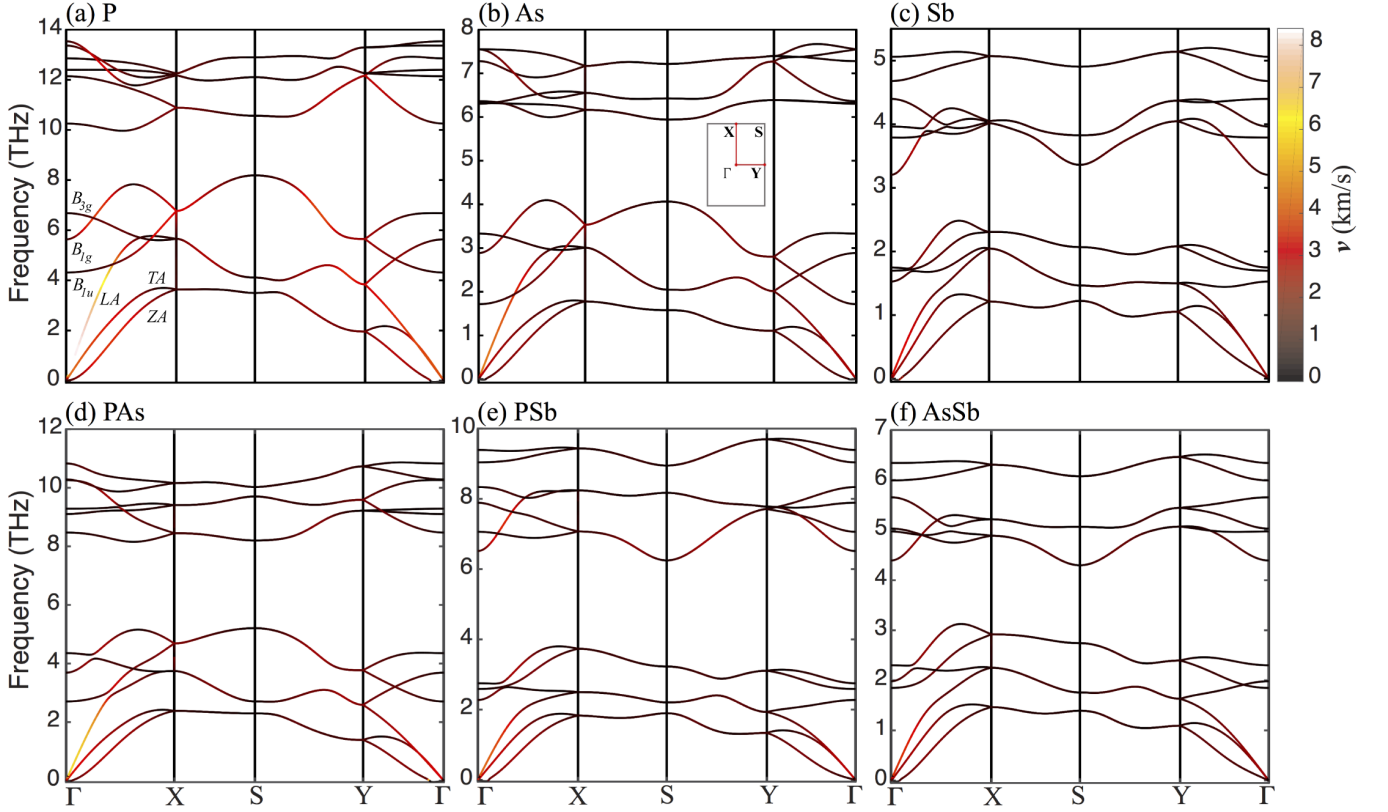


FIG. 2: Phonon dispersion curves together with group velocities (depicted as line color) along the high-symmetry directions of the first Brillouin zone.

duced atomic masses ($\mu = m_1 m_2 / (m_1 + m_2)$) for the alloy monolayers. When the bond stiffness becomes weaker (i.e. interatomic force constant becomes smaller) and the mass of atom becomes larger, the phonon frequencies shift to lower energies. Thus, the phonon branches become less disperse with exactly the same order, and v_{qi} of phonon modes markedly decrease with increasing the mass of constituent atom(s). In this context, the Debye temperature, calculated from the contributions of individual acoustic modes, $\theta_i = \hbar \omega_{i,max} / k_B$, as²⁹

$$\frac{1}{\theta_D^3} = \frac{1}{2} \left(\frac{1}{\theta_{LA}^3} + \frac{1}{\theta_{TA}^3} \right), \quad (1)$$

of P, As, Sb, PAs, PSb, and AsSb are predicted as follows, 206, 102, 74, 134, 101, and 84 K, respectively. For two-dimensional crystals Debye temperature is defined as follows³⁰,

$$\theta_D = \frac{\hbar v_s}{k_B} \left(\frac{4\pi n}{A} \right)^{1/2}, \quad (2)$$

where v_s is the sound velocity, n is the number of atoms in the unit-cell, and A is the area of the unit-cell³¹. Based on this formula we depict the square root of the unit cell area per number of atoms, $\delta^2 = A/n$, times Debye temperature (calculated from phonon dispersion via Eq.1)

with respect to inverse average atomic mass (total atomic mass over number of atoms in the unit cell, m/n) of the crystals. Quite nicely, the predicted Debye temperatures from our calculations follow the correlation with lattice constants and inverse of the average atomic mass as expected from Eq. (2). Note that, the sound velocity in the plot is considered as inversely proportional with average mass as it is in anharmonic crystals. The perfect linear correlation in Fig. 3 indicates that these systems might be quite anharmonic.

Phonon dispersion curves shown in Fig. 2 are not symmetric along the Γ -X-S and Γ -Y-S, giving rise to anisotropic phonon group velocities along the zigzag and armchair directions. In fact, all six monolayers have larger bond strength and Young's modulus in the zigzag direction as compared to the armchair direction, that induces anisotropic vibrational properties. Interestingly, the dispersion of acoustic modes along the ZZ and AC directions for antimonene is not so different as compared to phosphorene and arsenene, which would give rise to a smaller difference in thermal conductivity along the ZZ and AC directions. The predicted group velocities of LA modes of phosphorene along the ZZ and AC directions are in a good agreement with the previously reported first principles results (8.6 and 4.5 km/s)¹⁰ and experimental measurements (9.6 and 4.6 km/s)³² for bulk black phosphorus. Note that v_{qi} of major heat carrier

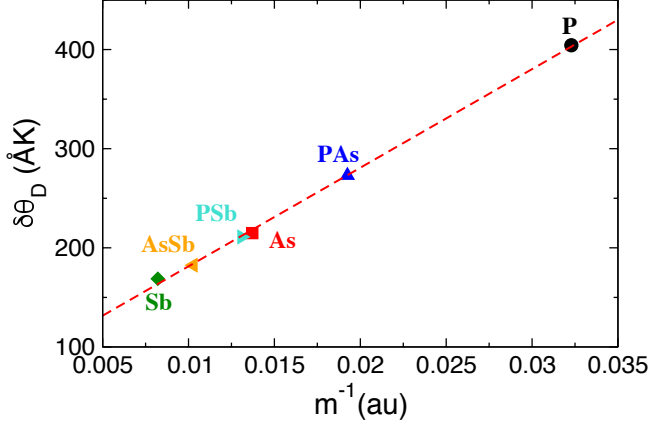


FIG. 3: $\delta\theta_D$ versus m^{-1} , where δ^2 , θ_D , and m are the area of the unit cell per atom, Debye temperature, and average atomic mass (total atomic mass over number of atoms in the unit cell) of each system, respectively.

phonon branches, i.e. acoustic modes, of arsenene and antimonene both along the ZZ and AC directions near the zone center are about two times smaller than those of black phosphorus. For instance, the group velocity values of LA modes at one third of $\Gamma - X$ point are 6.2, 3.6, 2.2, 4.3, 2.8, and 2.3 kms^{-1} for P, As, Sb, PAs, PSb, and AsSb, respectively. This notable difference in group velocity values of acoustic branches are fairly associated with the difference in κ values of the crystals. The predicted frequency gap between the low frequency and high frequency optical branches are 1.78, 1.85, 0.72, 2.95, 2.44, and 1.17 THz for P, As, Sb, PAs, PSb, and AsSb, respectively. Absent of a gap between the acoustic (a) and low frequency optical (o) phonons enhances three phonon processes (such as aoa , ooo and ooo) in puckered structures of present study. In fact, the lower thermal conductivity of puckered phosphorus versus buckled phosphorus is associated to the presence of a larger a - o gap in buckled one. Also, the significant effect of acoustic-optical phonon gaps on the aoa scattering channels is previously shown for different low dimensional materials^{9,33–35}. These above-mentioned three phonon processes may also affect the temperature dependence of κ since as temperature increases, number of optical phonons increase thereby enhancing three phonon processes involving optical phonons.

Subsequent to phonon dispersion analysis, we first calculate the lattice thermal conductivity of graphene in order to test our methodology and we predict it as $3290 \text{ Wm}^{-1}\text{K}^{-1}$ which is in quite good agreement with the literature^{36–39} (Details can be found in Supplementary Materials). Afterwards, we systematically investigate the lattice thermal transport properties of six group VA monolayer structures of P, As, Sb, PAs, PSb, and AsSb. The self-consistent solution of Peierls-BTE for lattice thermal conductivity (κ) of monolayers of the group VA elements as a function of temperature in the

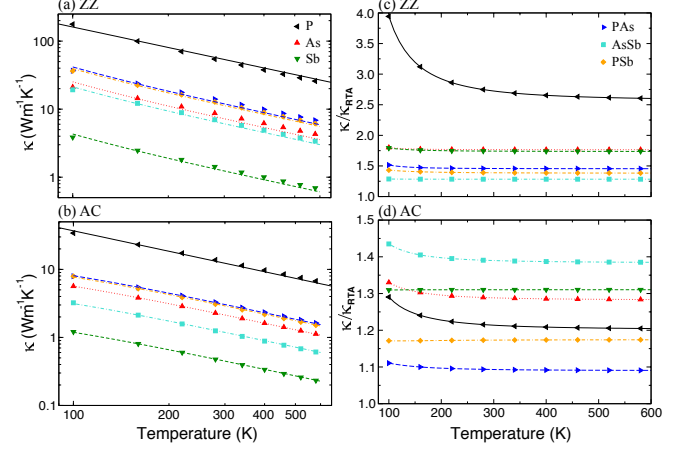


FIG. 4: Thermal conductivity of group VA monolayer crystals as a function of temperature along the (a) zigzag and (b) armchair directions calculated by the self-consistent solution of Peierls-BTE. Here, the ratio of the self consistent (κ) and zeroth order (corresponding to the RTA i.e. κ_{RTA}) solutions are also depicted for (c) zigzag and (d) armchair directions.

range from 100 K to 600 K are depicted with colored symbols in Fig. 4 (a) and (b). We find that all the monolayers exhibit obvious anisotropic thermal transport, which is attributed to the orientation dependent group velocities spotted in Fig. 2 and relaxation times. For instance, the room temperature κ along the zigzag (ZZ) direction is 3.94, 3.81, 2.99, 4.25, 4.14, and 5.58 times larger than that along the armchair (AC) direction for P, As, Sb, PAs, PSb, and AsSb, respectively. This behavior is consistent with the recent theoretical works^{9,10,40–42} carried out by using first-principles calculations, see Table I. Previously, the thermal conductivity of few layers black phosphorus films with a 15 nm thickness has been measured as 40 and $20 \text{ Wm}^{-1}\text{K}^{-1}$ and film with a 9.5 nm thickness has been measured² as 20 and $10 \text{ Wm}^{-1}\text{K}^{-1}$ along ZZ and AC directions, respectively. In addition, the thermal conductivity of a single crystal bulk black phosphorus has been measured⁴³ as 34 and $17 \text{ Wm}^{-1}\text{K}^{-1}$ along ZZ and AC directions, respectively. Even though we cannot directly compare the κ of a monolayer material with that of its few-layer and bulk form, our results for κ of phosphorene along both directions are in fair accordance with the previously reported experimental data for bulk and few-layer systems in terms of order of magnitude. Our calculated κ of phosphorene is higher than that for phosphorene film with a thickness of 9.5 nm. In a previous work, it was shown that the thermal conductivity of few-layer phosphorene does not vary much until the thickness of seven layers (4nm)⁴⁴. This behavior is quite different than graphene³⁶. This is due to fact that there is a much stronger interlayer interaction in black phosphorus due to overlap of interlayer wavefunctions rather than a pure van der Waals interaction^{45,46}. The thermal conductivity of phosphorene has been calculated by several groups. Interestingly, there is a huge

TABLE I: The calculated room temperature κ of the structures, together with the results reported in the literature. *a*, *b*, *c*, *d*, *e*, *f*, and *g* corresponds to the results extracted from Ref. 9, 40, 8, 41, 42, 10, and 47, respectively.

P		As		Sb	
κ_{ZZ}	κ_{AC}	κ_{ZZ}	κ_{AC}	κ_{ZZ}	κ_{AC}
50.68	12.88	8.16	2.14	1.33	0.44
112.5 ^a	24.1 ^a	26.1 ^a	5.6 ^a	8.4 ^a	4.1 ^a
30.2 ^b	13.6 ^b	30.4 ^c	7.8 ^c		
48.9 ^d	27.8 ^d				
110.0 ^e	36.0 ^e				
83.5 ^f	24.3 ^f				
15.3 ^g	4.6 ^g				

deviation between the calculated κ values. This can partially be attributed to different computational methods and computational parameters. In addition, Qin et. al. found that van der Waals interaction has a significant impact on the accurate description of the interatomic interactions in phosphorene. Inclusion of such dispersion interactions was found to decrease thermal conductivity of phosphorene⁴⁷.

We also find that ratio of κ along the ZZ and AC directions is almost temperature independent after 200 K and the maximum change corresponding to P is found to be $\sim 7\%$. Phosphorene has the largest κ along both directions among the six group VA monolayers within temperature range considered here, that can be partially correlated to the higher phonon group velocities in phosphorene. The order of κ is $P > PSb > PAs > As > AsSb > Sb$. The monolayers containing P has larger thermal conductivity as compared with the alloy ones without P atom. Sb monolayer has the lowest thermal conductivity for all temperatures considered here. The low κ value makes this material a promising candidate for future thermoelectric applications. On the other hand, the results clearly show that κ of black phosphorus can be tuned (reduced to enhance its thermoelectric potential) by alloying it with Sb, and also As doping even at very low concentrations^{37,48}, that will lead an opportunity to engineer these materials. This is because of the fact that substitutional As or Sb doping improves (suppresses) the electronic (thermal) transport by increasing (decreasing) the density of states around the Fermi level (band gap).

The zeroth iteration solutions of Peierls-BTE corresponding to RTA are also calculated. The ratio of the self consistent and RTA solutions for both ZZ and AC directions are depicted in Fig. 4 (c) and (d), respectively. For the crystals with strong Umklapp scattering, the room temperature κ calculated with the iterative solution is typically $<10\%$ greater than RTA solution⁴⁹. However, we predict that the iterative solution adds more than 10% to κ of all the crystals considered in our study, in both ZZ and AC directions. Interestingly, this difference to be considered as constant for the temperatures greater

than 200 K (which is larger than the θ_D of all the crystals except P), is significant particularly for κ of P along ZZ direction. This results clearly shows that the normal three-phonon processes play an important role in the considered crystals, especially in phosphorene. However, κ of all the structures is almost inversely proportional to temperature ($\kappa \sim T^{-1}$), indicating that phonon scattering mechanism is dominated by the Umklapp process.

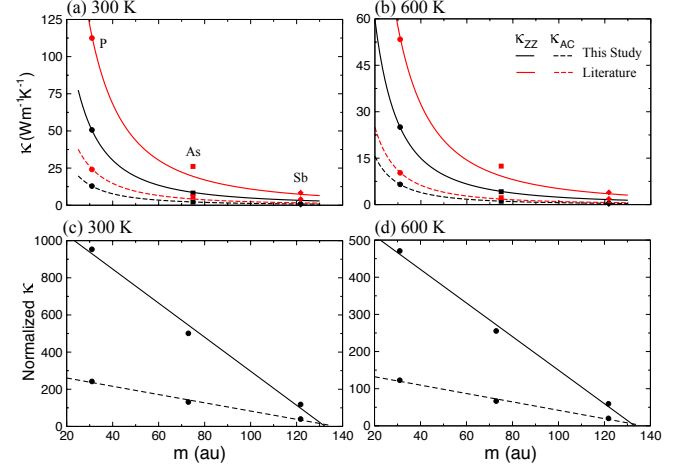


FIG. 5: Calculated κ of the P, As, and Sb based structures for (a) 300 and (b) 600 K temperature values, together with the results reported in Ref.9 and the normalized thermal conductivity, $\kappa/m\theta_D^3\delta$ for (c) 300 and (d) 600 K temperature values. Here, the black and red colors show the values calculated in this study and literature⁹. The solid and dashed styles correspond to the κ values along ZZ and AC directions.

Despite the apparent differences, such as group velocity and optical phonon gap values, in phonon dispersion of these materials there is an intriguing correlation between the κ of all the considered materials. Principally, single parameter function, $\kappa(T) = \alpha \times \kappa_{ref}(T)$ fits very well to calculated data for all the materials as seen in the fitting results depicted as lines in Fig. 4 (a) and (b), where α is a constant and $\kappa_{ref}(T)$ is the temperature dependent thermal conductivity of any reference system such as P (considered in fitting). Indeed, the thermal conductivity of all the considered materials are related to each other with a single parameter regardless of direction and temperature. In order to test the general validity of this correlation, we also apply the same fitting to recently published results for P, As, and Sb based structures by Zheng *et al.*⁹. In spite of the notable difference between our and their results seen in Table I, the function fits excellent to their calculations as well.

In addition, there is a distinct correlation between the κ of P, As, and Sb structures with atomic masses, m as $\kappa(m) = c/m^2$, where c is a constant, as represented in Fig.5 (a) and (b). Not surprisingly, the thermal conductivity values predicted by Zheng *et al.* (depicted as κ^*) also fits the function very well. Therefore, the decrease of κ of the pristine structures, P, As, and Sb, at

temperatures above 200 K follow a m^{-2} behavior. Slack suggested that the thermal conductivity is determined by four factors, including (1) average atomic mass, (2) interatomic bonding, (3) crystal structure and (4) size of anharmonicity⁵⁰. The first three factors determine harmonic properties. Three phonon scattering dominated κ can be given as

$$\kappa_s = A \frac{m\theta_D^3 \delta n^{1/3}}{\gamma^2 T} \quad (3)$$

where δ^2 is the unit-cell area per atom, n is the number of atoms in the unit cell, A is a constant given in terms of average Gruneisen parameter of modes, γ ²⁹, and m is the average atomic mass of the unit-cell. Inspired from the stated relation, we calculated the normalized thermal conductivity, $\kappa/m\theta_D^3\delta$ for 300 and 600 K as depicted in Fig. 5 (c) and (d) (Here, κ , m , δ , and θ_D are used in units of $\text{Wm}^{-1}\text{K}^{-1}$, au, m, and K, respectively). Surprisingly, these normalized values calculated for both ZZ and AC directions linearly decrease with the atomic mass. Within the Slack's approximation, this clearly points out the $A/\gamma^2 \propto m$ relation. As stated by Peng *et al.* the strong bonded crystals with light average mass possess a large θ_D^3 and thus a large $m\theta_D^3\delta$. The rest factor A/γ^2 in Eq. 3 is inversely related with the anharmonicity of crystal (small γ). Therefore, the calculated values clearly show that the size of anharmonicity increases from P- to Sb-based layered system.

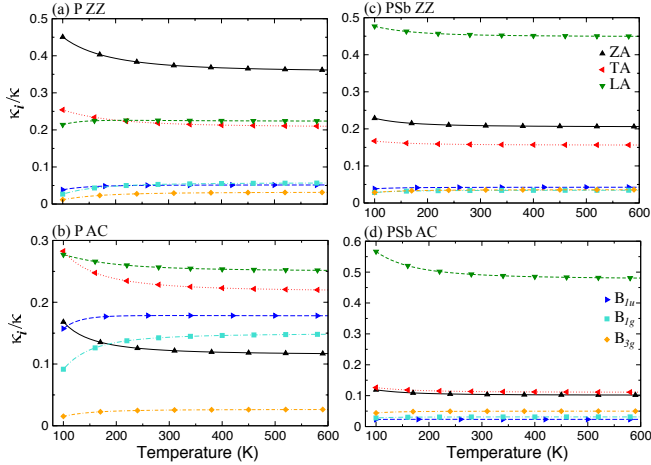


FIG. 6: Normalized contribution of acoustic and low frequency optical phonon branches to the thermal conductivity as a function of temperature along the zigzag and armchair directions of phosphorene and antimonene.

The ratio of thermal conductivity regarding to the three acoustic and three optical modes to total thermal conductivity, κ_i/κ (where $i = \text{ZA, LA, TA, B}_{1u}, \text{B}_{1g}, \text{and B}_{3g}$ and κ is total thermal conductivity) are determined for all the materials and the results for P and PSb are represented as an illustration in Fig. 6. The relative contribution of both acoustic and lowest three optical

phonons almost temperature independent for all the materials when the temperature is larger than the θ_D of all the crystals. In general, the total contribution of acoustic branches to κ is significantly higher than the contribution of optical modes. However, the lowest three optical modes, B_{1u} and B_{1g} have a notable contribution as seen in κ_{AC} of phosphorene. The proportion of LA mode notably higher than the rest for all the alloyed materials as seen in κ of PSb. Due to their non-planar structure, monolayers of group VA elements have significantly lower thermal conductivity as compared to graphene, 2000-5000 W/mK ^{36,37}. This can be partially attributed to the promoted phonon-phonon scattering of the out-of-plane acoustic (ZA) modes. Due to reflection symmetry perpendicular to graphene plane and hexagonal symmetry, three-phonon scattering involving ZA mode (anharmonic scattering of flexural phonons) process is significantly restricted in graphene^{38,39}. However such a symmetry is broken in group VA monolayers. Therefore, the selection rules, which are valid for graphene and suppress the phonon scattering, cannot be used for the puckered structures, thereby the anharmonic scattering is enhanced. In addition to their non-planar structure, the lower thermal conductivity of group VA monolayers is also due to the lower Debye temperature and smaller sound velocities as compared to graphene.

The ZA mode provides the largest contribution to the thermal conductivity along the zigzag direction of phosphorene while LA and TA modes dominate the thermal conductivity along the AC direction. Along the AC direction of phosphorene, the LA contribution exceeds the TA contribution when temperature is larger than 100 K. In graphene, however, the contribution of ZA mode to κ is 80% of total conductivity. In general, the contribution of the ZA mode to κ is smaller than 50% in group VA monolayers. In antimonene and phosphorene, the contribution of the ZA mode along the ZZ directions is substantially large as compared to the AC direction. The acoustic modes thermal conductivity is more than 70% of total thermal conductivity along the zigzag direction. Phosphorene and other group VA monolayers have been found to show superior structural flexibility along the armchair direction allowing it to have large curvatures. This mechanical flexibility is the origin of less dispersive ZA, LA and TA modes along that direction. The quadratic behavior of the ZA mode is more apparent along this direction with a smaller group velocities. Interestingly, alloying of phosphorene with As and Sb enhances (depresses) the contribution of the LA (ZA) modes to the thermal conductivity.

Since the calculated group velocities only provide a limited insight, we also investigate the effect of relaxation time on κ to have a better understanding of thermal conductivities. Besides phonon group velocities, the thermal conductivity is affected significantly by relaxation time, which is mainly determined by three-phonon processes as identified by the difference in above mentioned RTA results. Fig. 7 shows the calculated relaxation times corre-

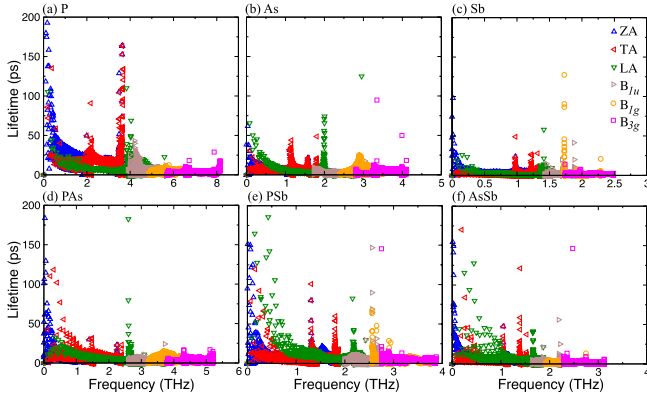


FIG. 7: Relaxation time of phonon modes as a function of frequency for acoustic and low frequency optical phonons at T=300K.

sponding to the three acoustic and three lowest frequency optical modes (ZA, LA, TA, B_{1u} , B_{1g} , and B_{3g}) of all the considered monolayer materials. There is a conspicuous difference between the relaxation times of acoustic phonons of P, As, and Sb based structures. In phosphorene, ZA and TA modes have long relaxation times (or low scattering rates) as compared to the other systems. In As and Sb monolayers, these modes undergo significant three phonon scatterings with much shorter relaxation times. However, the room temperature relaxation times for the alloy structures are found to be comparable with the P crystal in a wide range, in particular around low frequency region (0-1 THz). Nevertheless, due to their small group velocities, these monolayer have low thermal conductivity as compared to pristine P. This result is also supported by the mean free path (MFP) dependent thermal conductivity calculations depicted in Fig. 8. As clearly seen in Fig. 8, the mean free path of phonon modes of alloyed monolayer systems is following P based system. In contrast to graphene having significant contribution to κ from phonons with mean free paths of several microns⁵¹, phonons with MPF smaller than 100 nm contribute more than 90% of total thermal conductivity of P, As and Sb along the ZZ and AC directions. κ of Sb already reaches its maximum value before 100 nm. The center of distribution of mean free path (corresponding to 50% of cumulative κ) is 3 (2) nm for Sb, 11 (8) nm for As and 50 (23) nm for P along the ZZ (AC) direction. These values suggest that if the size of a group VA sheet is smaller than 50 nm, the κ of phosphorene significantly decreases due to boundary scattering. However, we can use much smaller As and Sb nanosheets without reducing thermal conductivity. It is interesting to note that the characteristic MFP of the Sb exhibits less anisotropy as compared to As and P. For alloy monolayers, phonons with larger mean free path also provides significant contribution to κ , meaning that we need to use larger size nanosheets as compared to pristine monolayers.

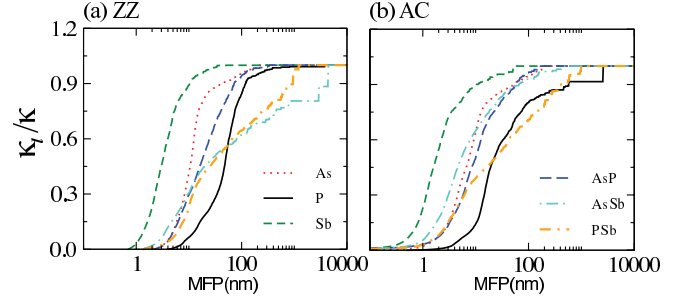


FIG. 8: Calculated cumulative thermal conductivity as a function of mean free path at T=300K along the (a) zigzag and (b) armchair directions.

IV. CONCLUSION

Owing to their anisotropic physical properties, group VA monolayers structurally similar to phosphorene offer a great potential for the electronic, optical and thermal device applications. In this respect, we investigate the thermal properties of six group VA monolayers. Firstly, all studied monolayers are found to have no negative frequencies in their phonon dispersions, indicating stability of these materials. Their puckered crystal structures give rise to significantly different relaxation times and phonon velocities along the ZZ and AC directions, thereby anisotropic thermal conductivity. We notice that atomic mass of constituent element(s) have a strong impact on thermal properties such that the thermal conductivities of P, As and Sb monolayers are inversely proportional to square of atomic mass. More interestingly, thermal conductivity of group VA monolayers can be very well described by a simple relation in terms of thermal conductivity of phosphorene, i.e. $\kappa(T) = \alpha \times \kappa_p(T)$, in the temperature range considered in this work. Thermal properties of phosphorene is tunable via substitutional Sb and As alloying. In other words, while the electronic properties enhances as a result of increase of density of states at the Fermi level, the thermal conductivity decreases. This property make these alloys promising candidate materials for thermoelectric applications. The thermal conductivity of all group VA monolayers is mainly dominated by acoustic phonons. Unlike graphene, the contribution of the ZA mode to κ is smaller than 50% in the group VA monolayers due to their puckered structures. While the contribution of ZA mode to the total thermal conductivity is quite large along the ZZ direction as compared to the AC direction, the LA mode is the main heat carrier along the AC direction.

V. ACKNOWLEDGEMENT

We acknowledge the support from Scientific and Technological Research Council of Turkey (TUBITAK-115F024). CS acknowledges the support from Anadolu

-
- * Electronic address: csevik@anadolu.edu.tr
- ¹ H. Liu, A. T. Neal, Z. Zhu, Z. Luo, X. Xu, D. Tománek, and P. D. Ye, *ACS Nano* **8**, 4033 (2014).
 - ² Z. Luo, J. Maassen, Y. Deng, Y. Du, R. P. Garrelts, M. S. Lundstrom, P. D. Ye, and X. Xu, *Nature Communications* **6**, 8572 (2015).
 - ³ S. Zhang, Z. Yan, Y. Li, Z. Chen, and H. Zeng, *Angewandte Chemie International Edition* **54**, 3112 (2015).
 - ⁴ D. Çakır, H. Sahin, and F. M. Peeters, *Phys. Rev. B* **90**, 205421 (2014).
 - ⁵ A. Chaves, T. Low, P. Avouris, D. Çakır, and F. M. Peeters, *Phys. Rev. B* **91**, 155311 (2015).
 - ⁶ D. Çakır, C. Sevik, and F. M. Peeters, *Phys. Rev. B* **92**, 165406 (2015).
 - ⁷ L. Li, Y. Yu, G. J. Ye, Q. Ge, X. Ou, H. Wu, D. Feng, X. H. Chen, and Y. Zhang, *Nat Nano* **9**, 372 (2014).
 - ⁸ M. Zeraati, S. M. Vaez Allaei, I. Abdolhosseini Sarsari, M. Pourfath, and D. Donadio, *Phys. Rev. B* **93**, 085424 (2016).
 - ⁹ G. Zheng, Y. Jia, S. Gao, and S.-H. Ke, *Phys. Rev. B* **94**, 155448.
 - ¹⁰ L. Zhu, G. Zhang, and B. Li, *Phys. Rev. B* **90**, 214302 (2014).
 - ¹¹ H. O. H. Churchill and P. Jarillo-Herrero, *Nat Nano* **9**, 330 (2014).
 - ¹² S. Wang, W. Wang, and G. Zhao, *Physical Chemistry Chemical Physics* **18**, 31217 (2016).
 - ¹³ G. Wang, R. Pandey, and S. P. Karna, *ACS Applied Materials and Interfaces* **7**, 11490 (2015).
 - ¹⁴ B. Peng, D. Zhang, H. Zhang, H. Shao, G. Ni, Y. Zhu, and H. Zhu, *Nanoscale*, (2017).
 - ¹⁵ D. Warschauer, *Journal of Applied Physics* **34**, 1853 (1963).
 - ¹⁶ S. Zhang, M. Xie, F. Li, Z. Yan, Y. Li, E. Kan, W. Liu, Z. Chen, and H. Zeng, *Angewandte Chemie* **128**, 1698 (2016).
 - ¹⁷ L. C. Hu, G. M. Ruan, T. C. Wei, C. J. Wang, Y. W. Lin, C. C. Lee, Y. Kawai, and T. T. Li, *Thin Solid Films* **570**, 574 (2014).
 - ¹⁸ G. Kresse and J. Hafner, *Phys. Rev. B* **47**, 558 (1993).
 - ¹⁹ X. Wu, D. Vanderbilt, and D. R. Hamann, *Phys. Rev. B* **72**, 035105 (2005).
 - ²⁰ R. W. Nunes and X. Gonze, *Phys. Rev. B* **63**, 155107 (2001).
 - ²¹ J. P. Perdew, K. Burke, and M. Ernzerhof, *Phys. Rev. Lett.* **77**, 3865 (1996).
 - ²² J. P. Perdew, K. Burke, and M. Ernzerhof, *Phys. Rev. Lett.* **77**, 3865 (1996).
 - ²³ H. J. Monkhorst and J. D. Pack, *Phys. Rev. B* **13**, 5188 (1976).
 - ²⁴ J. Ziman, *Electrons and Phonons: The Theory of Transport Phenomena in Solids* (Oxford University Press, 1960).
 - ²⁵ W. Li, J. Carrete, N. A. Katcho, and N. Mingo, *Computer Physics Communications* **185**, 1747 (2014).
 - ²⁶ W. Li, N. Mingo, L. Lindsay, D. A. Broido, D. A. Stewart, and N. A. Katcho, *Phys. Rev. B* **85**, 195436 (2012).
 - ²⁷ L. Lindsay, W. Li, J. Carrete, N. Mingo, D. A. Broido, and T. L. Reinecke, *Phys. Rev. B* **89**, 155426 (2014).
 - ²⁸ G. Qin, Q.-B. Yan, Z. Qin, S.-Y. Yue, H.-J. Cui, Q.-R. Zheng, and G. Su, *Scientific reports* **4**, 6946 (2014).
 - ²⁹ B. Peng, H. Zhang, H. Shao, Y. Xu, X. Zhang, and H. Zhu, *RSC Adv.* **6**, 5767 (2016).
 - ³⁰ C. Kittel, *Introduction to Solid State Physics*, 6th ed. (John Wiley & Sons, Inc., New York, 1986).
 - ³¹ B. Peng, D. Zhang, H. Zhang, H. Shao, G. Ni, Y. Zhu, and H. Zhu, *Nanoscale*, (2017).
 - ³² Y. Fujii, Y. Akahama, S. Endo, S. Narita, Y. Yamada, and G. Shirane, *Solid State Communications* **44**, 579 (1982).
 - ³³ L. Lindsay, D. A. Broido, and T. L. Reinecke, *Phys. Rev. Lett.* **111**, 025901 (2013).
 - ³⁴ L. Lindsay, D. A. Broido, and T. L. Reinecke, *Phys. Rev. Lett.* **109**, 095901 (2012).
 - ³⁵ A. Jain and A. J. H. McGaughey, *Journal of Applied Physics* **116**, 073503 (2014).
 - ³⁶ A. A. Balandin, *Nat. Mater.* **10**, 569 (2011).
 - ³⁷ J. Haskins, A. Kınacı, C. Sevik, H. Sevinçli, G. Cuniberti, and T. Çağın, *ACS Nano* **5**, 3779 (2011).
 - ³⁸ D. L. Nika and A. A. Balandin, *Reports on Progress in Physics* **80**, 036502 (2017).
 - ³⁹ D. L. Nika and A. A. Balandin, *Journal of Physics: Condensed Matter* **24**, 233203 (2012).
 - ⁴⁰ G. Qin, Q.-B. Yan, Z. Qin, S.-Y. Yue, M. Hu, and G. Su, *Phys. Chem. Chem. Phys.* **17**, 4854 (2015).
 - ⁴¹ T.-H. Liu and C.-C. Chang, *Nanoscale* **7**, 10648 (2015).
 - ⁴² A. Jain and A. J. H. McGaughey, *Scientific Reports* **5**, 8501 EP (2015).
 - ⁴³ Y. Wang, G. Xu, Z. Hou, B. Yang, X. Zhang, E. Liu, X. Xi, Z. Liu, Z. Zeng, W. Wang, and G. Wu, *Applied Physics Letters* **108**, 092102 (2016).
 - ⁴⁴ Y.-Y. Zhang, Q.-X. Pei, J.-W. Jiang, N. Wei, and Y.-W. Zhang, *Nanoscale* **8**, 483 (2016).
 - ⁴⁵ L. Shulenburg, A. Baczewski, Z. Zhu, J. Guan, and D. Tomanek, *Nano Letters* **15**, 8170 (2015), pMID: 26523860, <http://dx.doi.org/10.1021/acs.nanolett.5b03615>.
 - ⁴⁶ Z.-X. Hu, X. Kong, J. Qiao, B. Normand, and W. Ji, *Nanoscale* **8**, 2740 (2016).
 - ⁴⁷ G. Qin, X. Zhang, S.-Y. Yue, Z. Qin, H. Wang, Y. Han, and M. Hu, *Phys. Rev. B* **94**, 165445 (2016).
 - ⁴⁸ C. Sevik, H. Sevinçli, G. Cuniberti, and T. Çağın, *Nano Letters* **11**, 4971 (2011).
 - ⁴⁹ A. Ward, D. A. Broido, D. A. Stewart, and G. Deinzer, *Phys. Rev. B* **80**, 125203 (2009).
 - ⁵⁰ G. Slack, *Journal of Physics and Chemistry of Solids* **34**, 321 (1973).
 - ⁵¹ A. Cepellotti, G. Fugallo, L. Paulatto, M. Lazzeri, F. Mauri, and N. Marzari, *Nature Communications* **6**, 6400 EP (2015).